Advances in Aircraft and Spacecraft Science, *Vol. 7, No. 4 (2020) 353-369*
DOI: https://doi.org/10.12989/aas.2020.7.4.353

Flutter characteristics of axially functional graded composite wing system

L. Prabhu*[1] and J. Srinivas[2a]

[1]Department of Aerospace Engineering, Lakireddy Bali Reddy College of Engineering, Mylavaram, Krishna District, Andhra Pradesh – 521230, India
[2]Department of Mechanical Engineering, National Institute of Technology, Rourkela, Odisha – 769008, India

(Received October 27, 2019, Revised May 6, 2020, Accepted May 16, 2020)

Abstract. This paper presents the flutter analysis and optimum design of axially functionally graded box beam cantilever wing section by considering various geometric and material parameters. The coupled dynamic equations of the continuous model of wing system in terms of material and cross-sectional properties are formulated based on extended Hamilton's principle. By expressing the lift and pitching moment in terms of plunge and pitch displacements, the resultant two continuous equations are simplified using Galerkin's reduced order model. The flutter velocity is predicted from the solution of resultant damped eigenvalue problem. Parametric studies are conducted to know the effects of geometric factors such as taper ratio, thickness, sweep angle as well as material volume fractions and functional grading index on the flutter velocity. A generalized surrogate model is constructed by training the radial basis function network with the parametric data. The optimized material and geometric parameters of the section are predicted by solving the constrained optimal problem using firefly metaheuristics algorithm that employs the developed surrogate model for the function evaluations. The trapezoidal hollow box beam section design with axial functional grading concept is illustrated with combination of aluminium alloy and aluminium with silicon carbide particulates. A good improvement in flutter velocity is noticed by the optimization.

Keywords: aeroelastic tailoring; axial functional grading; cantilever wing; flutter boundary; firefly algorithm

1. Introduction

Aeroelastic instability in aircrafts is the most important threatening aspect resulting in the riding discomfort and final structural failure. Especially, for a highly flexible, long slender aircraft wing structures, the static divergence and dynamic flutter speeds are to be regularly monitored and controlled. Aircraft wing system subjected to active lift forces and moments has coupled bending-torsion motions. Dynamics of such a system is expressed in terms of plunge (bending) and pitch (twisting) displacements with self-excited lift force and pitching moments. The flutter speed can be enhanced remarkably by minimizing the inertial, elastic and aerodynamic coupling terms. The flutter requirements are to be satisfied at the initial design stages of wings itself. Several earlier

*Corresponding author, Associate Professor, E-mail: prabhulakshmananr@gmail.com
[a]Associate Professor, E-mail: srin07@yahoo.co.in

http://www.techno-press.org/?journal=aas&subpage=7 ISSN: 2287-528X (Print), 2287-5271 (Online)

studies focused on the use of composite materials for different kinds of wing designs. The structural properties of high aspect ratio composite wings were optimized by reducing the overall weight of the system (Liu and Lin 1991). The aeroelastic optimization of laminated swept composite wing structure was studied so as to achieve different system requirements (Weisshaar 1981). A procedure for enhancement of flutter stability in box type laminated composite wing system was given by Patil (1997). The ply lay-up, orientation and directional property of a composite wing were found to be the effective design parameters in improvement of flutter velocity (Wan *et al.* 2005, Guo *et al.* 2003, Qin and Librescu 2003). The flutter onset speed has increased considerably in composite laminated plate by maximizing the eigenfrequency that provoked the flutter (De Leon *et al.* 2012). It was found that the flutter boundary of the wing idealized as a composite beam under the follower force with engine mass was highly influenced by ply orientation (Amoozgar *et al.* 2013). The effect of crenellation parameters such as orientation, width and thickness of wings on the aeroelastic stability was addressed by Francois *et al.* (2017). In a more recent work, structural and aeroelastic responses like strength, mass, divergence etc. were optimized by selecting the lamination thickness of composite wing system (Dillinger *et al.* 2019).

A new class of composites known as functional graded materials (FGM) has attracted several research groups over the last decade because they can improve the structural and aerodynamic characteristics more effectively. This is possible by tailoring the continuous variations of material and geometric properties of the system along the thickness or axial directions. FGM have controlled volume distribution patterns inside the matrix phase. Librescu and Maalawi (2007) developed an analytical formulation to improve the aeroelastic stability of FGM wing by improving the torsional stability. Here, continuous linear, parabolic and piecewise volume distributions were employed. Dunning *et al.* (2014) presented Pareto optimization procedure of a functionally graded cantilever plate wing system made of two metallic substances. The aeroelastic instability region was identified with material and geometric grading and the effect of both on the stability boundary has been studied in the subsonic conditions. James *et al.* (2014) carried out the structural and aerodynamic optimization of box wing to achieve the maximum stable region and the result was compared with the sequential optimization. The natural frequencies of the structure have strong coherence with the flutter instability of structures. Maalawi (2011) presented optimum design of axially functional graded (AFG) continuous bar section to maximize its frequencies. The effect of material grading in thickness direction on the free vibration characteristics of both thin and thick walled box beam cross-sections was studied by Ziane *et al.* (2013). Tsiatas and Charalampakis (2017) illustrated the design of AFG beams and arches for maximizing the natural frequencies via differential evolution method. Asadi and Wang (2017) presented the effect of functional grading volume distributions along the thickness on the flutter boundaries in carbon nanotube reinforced composite beams. As an extension, Mehri *et al.* (2017) studied such a grading using conical curved panel subjected to aerodynamic and axial loads concurrently. Recently, Song *et al.* (2019) conducted optimal panel flutter analysis by axially varying the geometry and material parameters with the help of three arbitrary thickness functions.

In aerodynamic modeling and optimization, surrogate models are employed to minimize the computational cost of fluid dynamics. Sommerwerk *et al.* (2016) presented a surrogate model to replace computational fluid dynamics calculations in aircraft wings. Radial basis function (RBF) network with transient nonlinear computational data was used as training sets. Brouwer and McNamara (2020) proposed surrogate modeling to predict aeroelastic load in wing panel. Gao *et al.* (2019) considered the dynamic characteristics of FGM porous beams using surrogate

modeling. Optimization for required aerodynamic and structural features using efficient numerical schemes is another topic of interest. Burdette and Martins (2018) performed multi-point optimization of morphed wing system at different flight conditions.

For enhancement of flutter stability in aircraft wings made of FGM, several optimization criteria can be imposed. In the present work, the box beam hollow section of cantilever wing is considered as the load carrying structural member with axial functional graded distributions along the span. The dynamic equations are derived for coupled bending-torsional motion of wing using extended Hamilton's principle. The reduced order model is obtained from Galerkin's decomposition scheme and the resulting eigenvalue problem is solved to predict the flutter velocities. The parametric analysis is conducted to study the effect of important structural and geometrical parameters on the flutter velocity. Furthermore, the functional relationship between the output flutter velocity and input variables is generalized using radial basis function neural network model. After validating the network model with sufficient testing examples, it is used to estimate the flutter velocities for the optimization problem. In order to maximize the flutter velocity, new metaheuristic scheme known as firefly algorithm (FA) is employed. The structural mass is given as a constraint. The flutter boundary of optimized design is presented. Remaining part of the paper is organized as follows: section-2 describes the mathematical model of continuous wing system with plunge and pitching degrees of freedom for box beam section of wing. Further, the solution scheme and optimization problem are briefly described. In section-3, introduction to neural network model and firefly algorithm are presented. Section-4 explores the results and discussion of a case study of functionally graded wing section.

2. Mathematical modeling

A simplified model of FGM wing consists of a cantilever beam of variable cross-section and material properties.

2.1 Equations of motion

Fig. 1(a) shows the cantilever wing with sweep angle and taper effects. The axially functionally graded box beam section is shown in Fig. 1(b), which is the primary load carrying member of wing and other two parts (i) onward of the front spar and (ii) aft of rear spar are to give aerodynamic shape and are assumed to associate with mass and inertia terms. Therefore, the box beam portion alone is of interest.

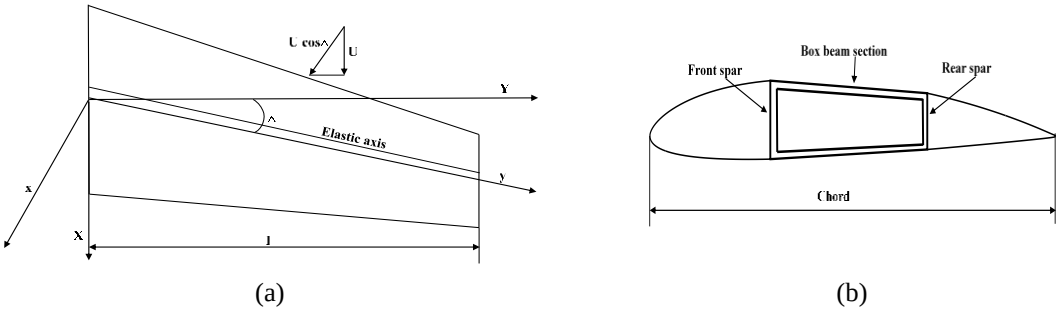

(a) (b)

Fig. 1 (a) Cantilever wing with sweep and taper and (b) box beam wing cross-section

The material properties of the trapezoidal box beam section are considered to vary continuously in the axial direction according to a non-negative power law index (Alshorbagy *et al.* 2011).

$$P(y)=(P_L-P_R)\left(1-\frac{y}{l}\right)^k+P_R \tag{1}$$

where P_R and P_L are the corresponding material properties at the right and left side of the beam, and k is the power law index.

The kinetic energy of tapered wing section in terms of plunge (h) and pitch (α) degrees of freedom and density $\rho(y)$ is given as:

$$T_W=\frac{1}{2}\int_0^l\left(\rho(y)A(y)\dot{h}^2+I_\alpha(y)\dot{\alpha}^2+2\rho(y)A(y)e\dot{h}\dot{\alpha}\right)dy \tag{2}$$

where $A(y)=A_0(y_c)^2$ and $I_\alpha(y)=I_{\alpha 0}(y_c)^4$ with A_0, $I_{\alpha 0}$, are area and mass moment of inertia at the root, while $y_c=1-\left(\frac{c_r-c_t}{c_r}\right)\left(\frac{y}{\ell}\right)$ is a taper factor chosen for convenience. Here, e is the distance between the elastic axis and centre of mass. The potential energy due to bending and torsion is expressed as

$$U_T=\int_0^l\left[AA\alpha'^2+BBh''^2\right]dy \tag{3}$$

where $AA=G(y)J(y)$ and $BB=E(y)I(y)$ are bending rigidity, and torsional rigidity respectively. Further, the variations in the energy terms are

$$\delta T_W=\int_0^l\left\{(y_c)^2\left(-m\ddot{h}-me\ddot{\alpha}\right)\delta h+(y_c)^2\left(-mI_{\alpha 0}(y_c)^4\ddot{\alpha}-me\ddot{h}\right)\delta\alpha\right\}dy \tag{4}$$

$$\delta U_T=\int_0^l\left\{-\left[(AA)'\alpha'+(BB)\alpha''\right]\delta\alpha+\left[(BB)''h''+2(BB)'h'''+(BB)h''''\right]\delta h\right\}dy \tag{5}$$

Here, again $m=\rho(y)A_0$ is mass per unit length and the dash over refers to the partial derivative with respect to y. The work done by aerodynamic forces is expressed as:

$$\delta W_A=\int_0^l\left(L\delta h+M\delta\alpha\right)dx \tag{6}$$

where L and M are the quasi-steady aerodynamic lift and moment terms which are defined in terms of sweep angle (Λ) as (Mazidi and Fazelzadeh 2010):

$$\begin{aligned}L=&\pi\rho_\infty b^2(y_c)^2\left[-\ddot{h}+U\cos\Lambda\dot{\alpha}-U\sin\Lambda\dot{h}'-b(y_c)a\left(\ddot{\alpha}+U\sin\Lambda\dot{\alpha}'\right)\right]\\&+Cl_\alpha\rho_\infty Ub(y_c)\cos\Lambda\left[-\ddot{h}+U\cos\Lambda\alpha-U\sin\Lambda h'+b(y_c)\left(\frac{1}{2}-a\right)\left(\dot{\alpha}+U\sin\Lambda\alpha'\right)\right]\end{aligned} \tag{7}$$

$$M = Cm_\alpha \rho_\infty Ub(y_c)\cos\Lambda\left[-\ddot{h} + U\cos\Lambda\alpha - U\sin\Lambda h' + b(y_c)\left(\frac{1}{2}-a\right)\left(\dot{\alpha} + U\sin\Lambda\dot{\alpha}'\right)\right]$$
$$+\pi\rho_\infty b^3(y_c)^3\left[U\left(\frac{1}{2}-a\right)\dot{\alpha}\cos\Lambda + \frac{1}{2}U^2\cos\Lambda\sin\Lambda\alpha' - a\ddot{h} - Ua\dot{h}' + b(y_c)\left(\frac{1}{8}+a^2\right)\left(\ddot{\alpha} + U\sin\Lambda\dot{\alpha}'\right)\right] \quad (8)$$

where *a, b,* and *U* are the non-dimensional distance of elastic axis from mid-chord, semi-chord and freestream velocity respectively.

The extended Hamilton's principle can be written as:

$$\int\left(\delta T_W - \delta U_T + \delta W_A\right)dt = 0 \quad (9)$$

By substituting Eqs. (4)-(6) in Eq. (9), the following equations of motion are obtained:

$$my_c^2\ddot{h} + my_c^2 e\ddot{\alpha} + \left[BB''h'' + 2BB'h''' + BBh''''\right] = L \quad (10)$$

$$I_{\alpha 0}y_c^4\ddot{\alpha} + my_c^2 e\ddot{h} - \left[AA'\alpha' + AA\alpha''\right] = M \quad (11)$$

The variable *h* and *t* are made dimensionless by using *l* and characteristic time $\sqrt{ml^4/EI}$ (inversely proportional to systems natural frequency). Now, the dependent variables and system parameters are non-dimensionally written as:

$$h^* = \frac{h}{l},\quad I_y^* = \frac{I_y}{ml^2},\quad U^* = \frac{U}{\sqrt{EI/ml^2}},\quad b^* = \frac{b}{l},\ t^* = t\Big/\sqrt{ml^4/EI},\quad \mu = \frac{\pi\rho b^2}{m},\quad e^* = \frac{e}{l}$$

2.2 Solution of dynamic equations

To obtain the solution of these aeroelastic equations, an approximation technique using Galerkin's method (Fletcher 1984) is employed. The variables *h* and *α* in Eqs. (10) and (11) are expressed in terms of modal functions as (Hodges and Pierce 2011):

$$h(\eta,t) = \sum_{i=1}^{\infty} W_i(\eta)r_i(t) \quad (12)$$

$$\alpha(\eta,t) = \sum_{i=1}^{\infty} A_i(\eta)s_i(t) \quad (13)$$

The modal functions of cantilever end conditions are given as:

$$W_i(\eta) = \cosh(\beta_i\eta) - \cos(\beta_i\eta) - \sigma_i\left[\sinh(\beta_i\eta) - \sin(\beta_i\eta)\right] \quad (14)$$

$$A_i(\eta) = \sqrt{2}\sin(\gamma_i\eta) \quad (15)$$

with,

$$\sigma_i = \frac{\cosh(\beta_i) + \cos(\beta_i)}{\sinh(\beta_i) + \sin(\beta_i)} \tag{16}$$

where $\eta = y/l$ and β_i is a non-dimensional frequency parameter. By substituting the user defined number of modes i into equations of motion and applying the Galerkin's technique, the reduced set of differential equations in time domain are obtained, which can be written in a matrix form as:

$$[M]\ddot{q} + [C]\dot{q} + [K]q = 0 \tag{17}$$

where, [M], [C], [K] are the mass, damping, and stiffness matrix respectively, while $q = \{r_i \quad s_i\}^T$ is a displacement vector. The equations are further transformed into state-space form as:

$$\dot{Q} = [A]Q \tag{18}$$

where, $Q = \{q \quad \dot{q}\}^T$ is resultant displacement vector and $[A] = \begin{bmatrix} [0] & [I] \\ -[M]^{-1}[K] & -[M]^{-1}[C] \end{bmatrix}$ is the system matrix. The eigenvalues obtained from the system matrices have real and imaginary parts respectively representing damping coefficients and the natural frequencies. The flutter speed (U_f) is identified as the flow velocity at which a real part of eigenvalue changes its sign.

2.3 Formulation of optimization

In order to achieve an optimal box section for the wing, the optimization problem is formulated as:

$$\text{Maximize } f(X) = U_f \tag{19}$$

subjected to

$$g(X) = \frac{m(X)}{m_t} - 1 \le 0 \tag{20}$$

with $X \in [x_1, ..., x_n]^T \ \forall \ x_i \in [x_i^{\min}, x_i^{\max}], i = 1,2,...n$, are the design variables which include geometric and material parameters. Here, m_t is the scaling maximum mass of the wing.

3. Present approach

Artificial neural networks are widely used in several engineering applications today as surrogate models, where the experimental and computational difficulties are involved in the system. Radial basis function is one kind of function-approximation supervised neural networks (Guan *et al.* 2016) and has an advantage of limited network parameters along with good reliability in output performance. The RBF is a feed-forward three-layer network with input, output and radial basis (hidden) layers making use of nonlinear radial basis activation functions. Fig. 2 shows the block diagram of the RBF.

The hidden nodes are not weighed from the input side, however, each hidden node receives a central vector radially. The sum of the weighted outputs at a hidden layer is defined as:

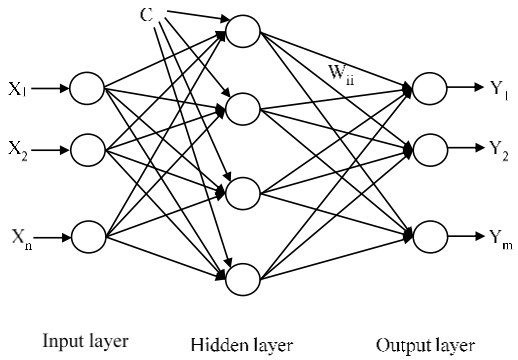

Fig. 2 RBF neural network topology

$$Y(X) = W\varphi(X, C) \tag{21}$$

where X is the input vector, W is connection weight from hidden nodes to outputs, C is a central vector, and φ is radial basis function which in most of the cases is a Gauss function defined by:

$$\varphi(X, C) = G(\|X - C\|) = \exp\left(-\frac{1}{\sigma^2}\|X - C\|^2\right) \tag{22}$$

where σ represents the width or spread factor and the central vectors are usually selected as subsets of input vector for simplicity. Thus, during the training process, a correct set of connection weights W are obtained to achieve the outputs Y close to the target values.

To achieve the optimal geometry of the box section, a non-conventional firefly optimization scheme is employed.

3.1 Firefly optimization algorithm

Firefly algorithm is a metaheuristic optimization scheme, which is based on the flashing nature of fireflies. FA is employed to group the parts based on their similarities (Sayadi *et al.* 2013). FA was used effectively to solve a constrained optimization problems in several engineering applications. The algorithm is framed based on three simple rules (Basu and Mahanti 2012, Shukla and Singh 2017):

1. All fireflies are unisex so that one will be attracted to other irrespective of their sex.
2. Attractiveness is proportional to brightness, so less bright firefly will move towards the brighter one. However, the light intensity (I_i) (apparent brightness) is inversely proportional to distance between the fireflies (r_{ij}).
3. The brightest one move randomly as no other firefly is to attract it.

The brightness should be associated with objective function of the system. The pseudo-code of firefly algorithm based on above rules is given below:

Begin
Objective function f(x), $x=(x_1,\ldots,x_n)^T$
Generate initial population of fireflies x_i $(i=1,2,\ldots,n)$
Light intensity I_i, at x_i is determined by $f(x_i)$

Define light absorption coefficient γ
While *(t<Max Generation)*
for *i=1:n all n fireflies*
for *j=1:d loop over all d dimensions*
If *(I_i<I_j), Move firefly i towards j; end if*
Vary attractiveness with distance r via exp(-γr^2)
Evaluate new solutions and update light intensity
end for *j*
end for *i*
Rank the fireflies and find the current global best
end while
Post process results and visualization
End

The I_i decreases as r_{ij} increases and additionally, the air absorbs light which further reduces the value of I_i as the distance increases. So the light intensity is defined as:

$$I_i\left(r_{ij}\right) = I_0 \exp\left(-\gamma r_{ij}^2\right) \tag{23}$$

where I_0 is intensity at r_{ij} is zero and γ is light absorption coefficient. Attractiveness (β) is proportional to I_i seen by adjacent fireflies and it is given as

$$\beta = \beta_0 \exp\left(-\gamma r_{ij}^2\right) \tag{24}$$

Also, β_0 is attractiveness at r_{ij}=0. The movement of firefly is based on the attractiveness and the firefly *i* is being moved towards the brighter firefly *j* as

$$x_i^{t+i} = x_i^t + \Delta x_i \tag{25}$$

where

$$\Delta x_i = \beta_0 \exp(-\gamma r_{ij}^2)(x_j^t - x_i^t) + \kappa \varepsilon_i \tag{26}$$

Here, κ and ε_i are the parameter controlling the step size and random vector respectively. To obtain the optimum solution using the constraint in the firefly algorithm, selection criteria are to be incorporated based on the feasibility to narrow down the search into the feasible region.

In present context, initially random population of design variables is generated and the function estimation is performed with trained neural network model, which is called surrogate model. By applying various steps in FA, the initial population is updated successively based on the function values of a population. The procedure is repeated till convergence is achieved.

4. Numerical simulations

The coupled analysis program and optimization modeling are implemented in Matlab. By suitably selecting the number of modes, the resultant matrix sizes are decided. Initially, the flutter speed of straight clean wing geometry is obtained. It is found as 27.1 m/s which is close to the value 26.35 m/s obtained earlier (Abbas *et al.* 2008). For FGM analysis, the materials used are

Table 1 Material properties (Dunning *et al.* 2014)

Property	Al-alloy	AlSiC
Density (kg/m^3)	2768	2800
Young's modulus (Gpa)	69	107
Poisson's ratio	0.33	0.33

Table 2 System parameters

Parameter of wing	Value
Chord (c)	0.15 m
Semi chord (b)	0.075 m
Span (l)	1 m
Centre of mass (Xcg)	49.9491% of chord
Wing mass (m)	0.6972 kg/m
Elastic axis (a)	48.2569% of chord
Mass moment of inertia (I_y)	0.0041 kg/m
Bending stiffness (EI) AlSiC	475.1336 Nm^2
Bending stiffness (EI) Al-alloy	306.3945 Nm^2
Torsional stiffness (GJ) AlSiC	801.097 Nm^2
Torsional stiffness (GJ) Al-alloy	516.5417 Nm^2
Cl_α	2π
$Cm_{\alpha 0}$	-0.125

aluminium alloy (Al-alloy) and aluminium with silicon carbide particulates (AlSiC). The material data considered is depicted in Table 1.

The stability region of the straight untapered wing is determined using the geometric data given in Table 2.

The width of the box beam section considered for flutter study is 18% of chord and the front spar is located at 43% of chord. The flutter velocities for wing system made of AlSiC and Al-alloy are found independently as 48.95 m/s and 39.31 m/s respectively via the eigenvalue prediction approach.

4.1 Influence of geometrical parameters and AFG on the stability boundary

The parametric study is conducted to predict the most influencing parameters on the flutter speed. The geometrical and material parameters taken into account in this study are sweep angle (SA), mass centre position from leading edge (Xcg), thickness of the box beam (TH), taper ratio (TR) and power law index (PL). The bounds of the geometrical parameter considered are shown in Table 3. The power law index is varied from zero.

The density of both the materials is almost similar, so the average density is considered as the constant in this analysis. The study is carried out with AlSiC and Al-alloy at the left and right sides respectively as depicted in Fig. 3.

Table 3 Parametric bounds

	Parameters			
	SA in deg	**TR**	**TH in m**	**Xcg × 100 in %**
Case 1	0 to 50	0.5 to 1	0.02	0.49949
Case 2	0	0.5 to 1	0.02	0.485 to 0.49949
Case 3	0	1	0.01 to 0.02	0.485 to 0.49949

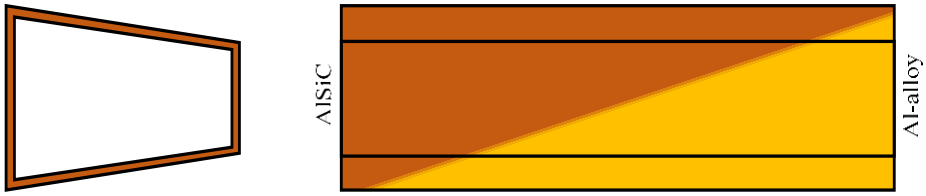

Fig. 3 Axial material grading: AlSiC at left and Al-alloy to the right

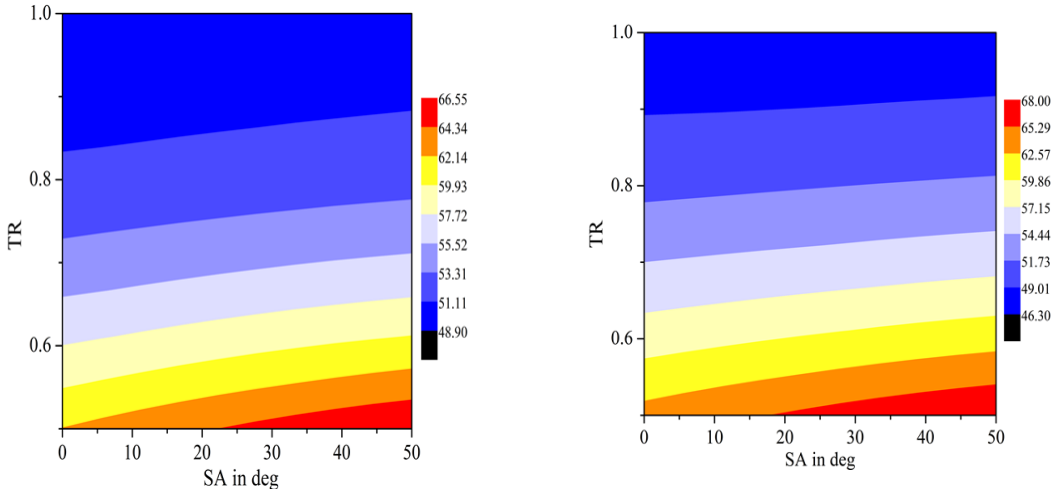

(a) PL = 0 (b) PL = 0.5

(c) PL = 1 (d) PL = 2.5

Fig. 4 Contour plots of flutter velocities against SA and TR

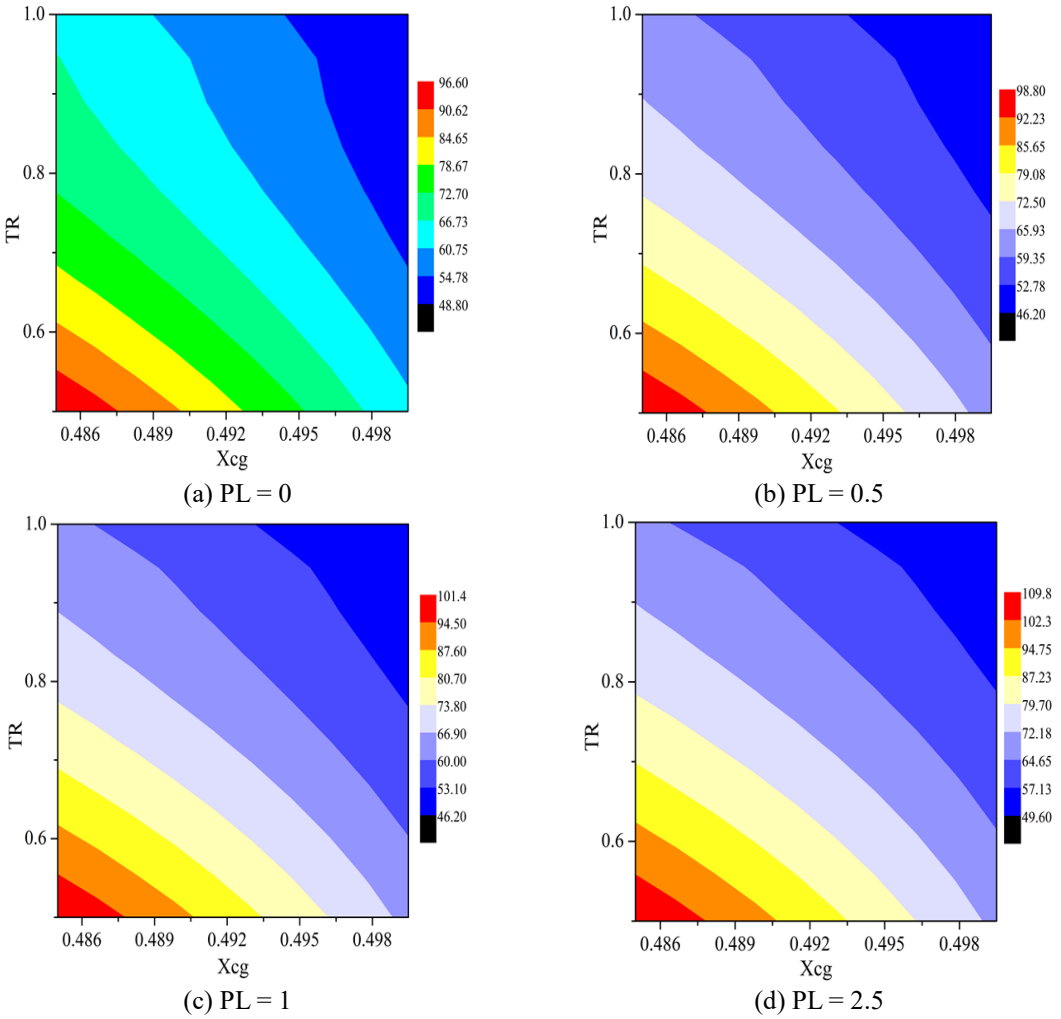

(a) PL = 0 (b) PL = 0.5

(c) PL = 1 (d) PL = 2.5

Fig. 5 Variation of flutter velocities against Xcg and TR

Case 1: The instability boundary for the range of parameters SA and TR is identified by maintaining a constant TH and Xcg and is shown in Fig. 4. For PL value equal to zero, the flutter boundary increases proportional to SA and inversely proportional to TR. When PL is increased to 0.5, the flutter velocity decreases till TR = 0.8 and then the flutter boundary increases.

For PL = 1, the same trend is observed, but the flutter velocities are found to be higher than the PL = 0.5 case. From Fig. 4, for PL = 2.5, the flutter boundary is found to be well enhanced compared to PL = 0, 0.5, and 1. For all TR values, the flutter velocity is increasing as the SA increases and the same is observed for all PL values. This shows the sweep angle is the dominant parameter over flutter instability.

Case 2: In this case, the effect of centre of mass and taper ratio on the flutter instability is studied with TH and SA as constant. For a wing, the flutter boundary is enhancing as the Xcg is moved towards the leading edge and TR is decreased. When the blending of materials comes into the picture, the enhancement of flutter velocity follows the same trend as in case 1. Here the flutter

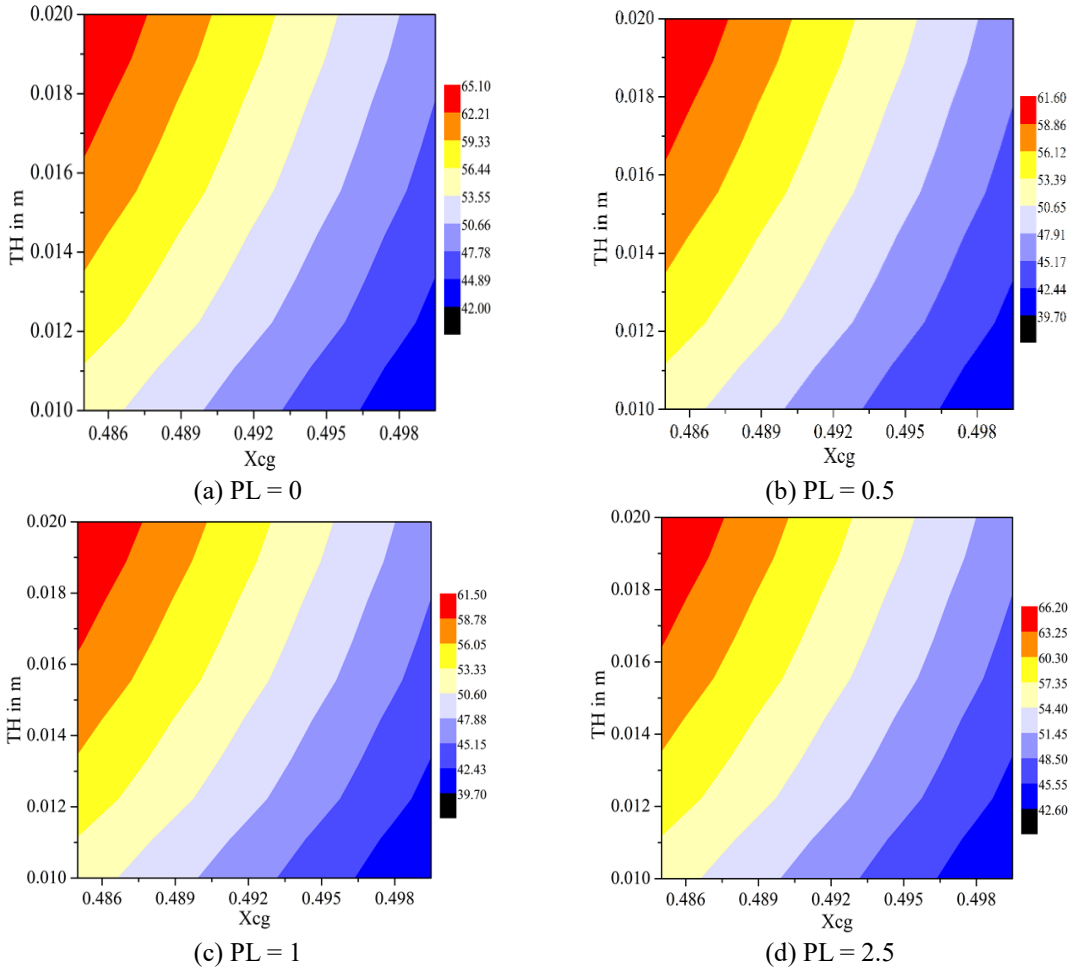

(a) PL = 0 (b) PL = 0.5

(c) PL = 1 (d) PL = 2.5

Fig. 6 Variation of flutter velocities against Xcg and TH

boundary has increased drastically compared to TR against SA as shown in Fig. 5. From case 2 results, Xcg is found to be the dominant parameter compared to SA and TR.

Case 3: The effect of thickness of the box beam section is important on the flutter velocity. The variable parameters in this case are TH and Xcg. The flutter velocity increases as Xcg distance decreases (from the leading edge) and TH value increases. For PL values 0.5 and 1, the flutter boundary diminishes compared to PL = 0, but for PL = 2.5 the flutter boundary is augmented as shown in Fig. 6. Again the Xcg is a dominant parameter compared to TH.

4.2 Surrogate model

The training sets consist of SA, TR, TH, Xcg, and PL as input and U_f as output. The spread parameter is set as 1 and the Matlab toolbox is used for training with 1010 training sets. The output computed versus target values is shown in Fig. 7. The flutter velocity obtained from trained RBF for different configurations are depicted in Table 4.

Table 4 Comparison of RBF and analytical flutter velocities

SA in deg	TR	TH in m	Xcg x 100 in %	PL	RBF-U_f in m/s	Analytical-U_f in m/s
27.3246	0.075	0.0175	0.485	2.71226	104.23	103.28
18.6695	0.0705	0.0176	0.485	1.8211	101.58	102.83

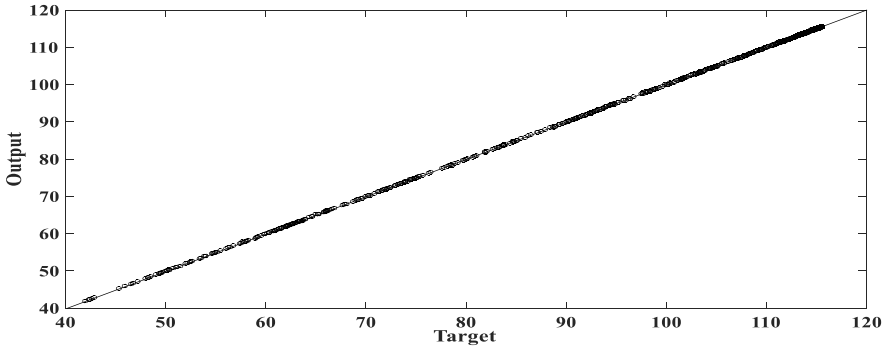

Fig. 7 Regression plot

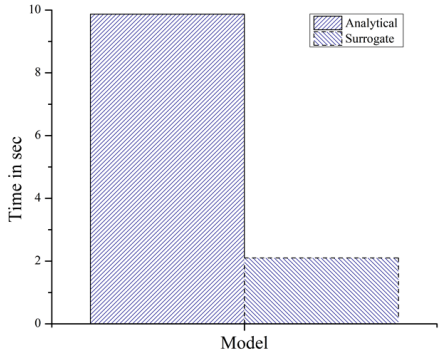

Fig. 8 Computational time

The average error in output of trained surrogate model and the analytical method are in the acceptable range. The computational time of the analytical and surrogate model is 9.87 and 2.1 seconds respectively as shown in Fig. 8.

4.3 Optimized configuration

By using the trained neural network model, the objective function is evaluated for every individual in the population during firefly implementation. The main motive is to reduce the mass of the wing without compromising the flutter boundary. The initial desired weight of the wing is selected as 0.61 kg. Initially, 20 fireflies are generated randomly within the bounds and their aeroelastic characteristics are evaluated. The penalty approach is used to handle the constraints with an effective objective function according to $f'(X) = f(X) + R\varphi(g(X))$, where $\varphi(g(X))$ is the penalty function. Also, R is a high penalty value, which is here taken as 10,000. Here, a vector of design variables $X \in [SA \quad TR \quad TH \quad Xcg \quad PL]$. The penalty function is taken as

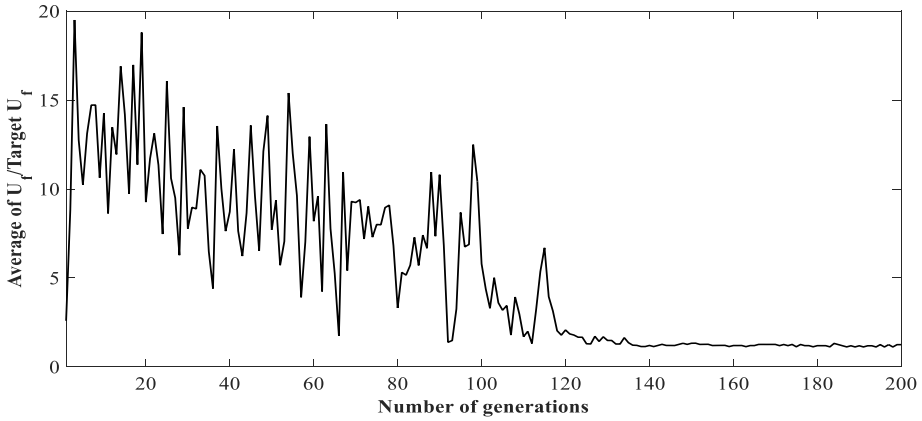

Fig. 9 Fitness convergence trend

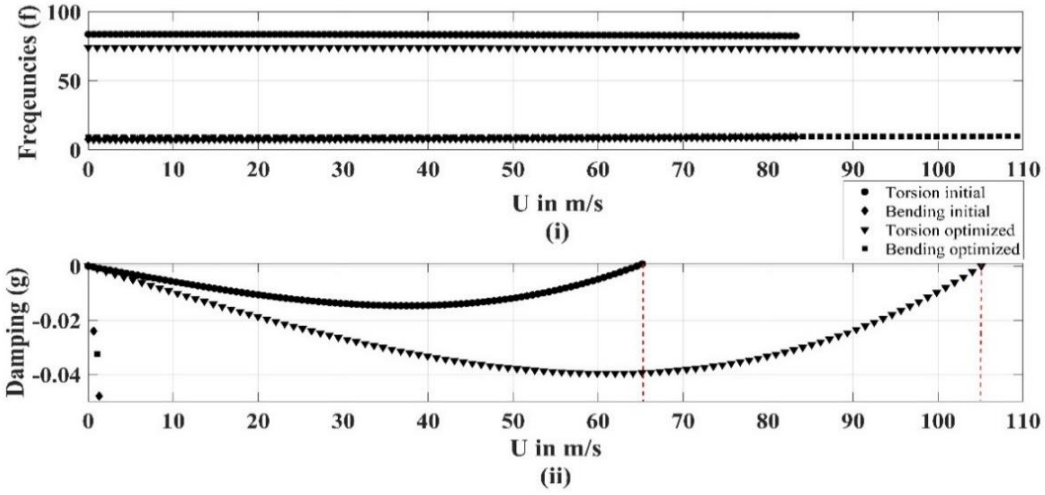

Fig. 10 (i) Velocity-frequency (U-f) plot and (ii) velocity-damping (U-g) plot of initial and optimized wing

$$\varphi(g(X)) = \begin{cases} \left(\dfrac{m(x)}{0.61} - 1\right) & for\ g(X) > 0 \\ 0 & otherwise \end{cases} \tag{27}$$

After several trials, the following parameters of firefly optimization are considered: γ = 1 and α = 0.25. The lower and upper bounds of the five variables selected are $SA \in [0 \quad 50]$ degrees, $TR \in [0.5 \quad 1]$, $TH \in [0.01 \quad 0.02]$ m, $Xcg \in [0.485 \quad 0.49949]$, $PL \in [0 \quad 5]$. The error convergence is shown in Fig. 9.

The initial parameters before optimization are SA = 44.4°, TR = 0.075, TH = 0.02 m, Xcg = 49.94% of chord, and PL = 0.5, while the optimized parameters predicted are SA = 27.7714°, TR = 0.075, TH = 0.0177 m, Xcg = 48.5% of chord and PL = 2.8745. The corresponding flutter velocity identified by RBF neural network is 108.41 m/s which is higher than the initial

flutter velocity of 67.6 m/s. Furthermore, the actual values of flutter speeds with the analytical method are found to be 64.55 m/s and 105.1 m/s respectively as seen in Fig. 10 where the damping term (real part) changes sign. Therefore, the approach is reliable.

5. Conclusions

The aeroelastic characteristics of a cantilever wing made up of axially functional graded box beam cross-section was studied in detail. The equations of motion of the system with continuously varying material and geometrical properties were derived. The numerical results show that geometric parameter mass center position from leading edge Xcg is the most influencing out of all five selected design parameters. The flutter boundary shrinks with lower power law indices (0.5, 1) compared to the PL = 0. Flutter onset increases as the TR decreases and Xcg moves towards the leading edge. Flutter velocity was proportional to the thickness of the box beam and sweep angle of the wing. For AFG wing, the stable zone has improved as compared to the base materials. The radial basis function in conjunction with firefly optimization algorithm effectively maximizes the flutter velocity under mass constraint. The 3-D model of the optimized wing section in the air stream is to be tested in order to identify the changes in natural frequencies as a function of freestream velocity.

References

Abbas, L.K., Chen, Q., Marzocca, P. and Milanese, A. (2008), "Non-linear aeroelastic investigations of store(s)-induced limit cycle oscillations", *P. I. Mech. Eng. Part G J. Aer.*, **222**(1), 63-80. https://doi.org/10.1243/09544100JAERO241.

Alshorbagy, A.E., Eltaher, M.A. and Mahmoud, F.F. (2011), "Free vibration characteristics of a functionally graded beam by finite element method", *Appl. Math. Model.*, **35**(1), 412-425. https://doi.org/10.1016/j.apm.2010.07.006.

Amoozgar, M.R., Irani, S. and Vio, G.A. (2013), "Aeroelastic instability of a composite wing with a powered-engine", *J. Fluids Struct.*, **36**, 70-82. https://doi.org/10.1016/j.jfluidstructs.2012.10.007.

Asadi, H. and Wang, Q. (2017), "An investigation on the aeroelastic flutter characteristics of FG-CNTRC beams in the supersonic flow", *Compos. Part B Eng.*, **116**, 486-499. https://doi.org/10.1016/j.compositesb.2016.10.089.

Basu, B. and Mahanti, G.K. (2012), "Thinning of concentric two-ring circular array antenna using firefly algorithm", *Scientia Iranica*, **19**(6), 1802-1809. https://doi.org/10.1016/j.scient.2012.06.030.

Brouwer, K.K. and McNamara, J.J. (2020), "Surrogate-based aeroelastic loads prediction in the presence of shock induced-separation", *J. Fluid. Struct.*, **93**, 102838. https://doi.org/10.1016/j.jfluidstructs.2019.102838.

Burdette, D.A. and Martins, J.R.R.A. (2018), "Design of a transonic wing with an adaptive morphing trailing edge via aerostructural optimization", *Aerosp. Sci. Technol.*, **81**, 192-203. https://doi.org/10.1016/j.ast.2018.08.004.

De Leon, D.M., de Souza, C.E., Fonseca, J.S.O. and da Silva, R.G.A. (2012), "Aeroelastic tailoring using fiber orientation and topology optimization", *Struct. Multidisciplin. O.*, **46**, 663-677. https://doi.org/10.1007/s00158-012-0790-8.

Dillinger, J.K.S., Abdalla, M.M., Meddaikar, Y.M. and Klimmek, T. (2019), "Static aeroelastic stiffness optimization of a forward swept composite wing with CFD-corrected aero loads", *CEAS Aeronaut. J.*, **10**(4), 1015-1032. https://doi.org/10.1007/s13272-019-00397-y.

Dunning, P.D., Stanford, B.K., Kim, H.A. and Jutte, C.V. (2014), "Aeroelastic tailoring of a plate wing with

functionally graded materials", *J. Fluid. Struct.*, **51**, 292-312. https://doi.org/10.1016/j.jfluidstructs.2014.09.008.
Fletcher, C.A.J. (1984), *Computational Galerkin Methods*. Springer, Berlin, Heidelberg, Germany.
Francois, G., Cooper, J.E. and Weaver, P.M. (2017), "Aeroelastic tailoring using crenellated skins-modelling and experiment", *Adv. Aircraft Spacecraft Sci.*, **4**(2), 93-124. http://doi.org/10.12989/aas.2017.4.2.093.
Gao, K., Li, R. and Yang, J. (2019), "Dynamic characteristics of functionally graded porous beams with interval material properties", *Eng. Struct.*, **197**, 109441. https://doi.org/10.1016/j.engstruct.2019.109441.
Guan, X., Zhu, Y. and Song, W. (2016), "Application of RBF neural network improved by peak density function in intelligent color matching of wood dyeing", *Chaos Solitons Fract.*, **89**, 485-490. https://doi.org/10.1016/j.chaos.2016.02.015.
Guo, S.J., Bannerjee, J.R. and Cheung, C.W. (2003), "The effect of laminate lay-up on the flutter speed of composite wings", *P. I. Mech. Eng. Part G J. Aer.*, **217**(3), 115-122. https://doi.org/10.1243/095441003322297225.
Hodges, D.H. and Pierce, G.A. (2011), *Introduction to Structural Dynamics and Aeroelasticity*, Cambridge University Press, Cambridge, U.K.
James, K.A., Kennedy, G.J. and Martins, J.R.R.A. (2014), "Concurrent aerostructural topology optimization of a wing box", *Comput. Struct.*, **134**, 1-17. https://doi.org/10.1016/j.compstruc.2013.12.007.
Librescu, L. and Maalawi, K. (2007), "Material grading for improved aeroelastic stability in composite wings", *J. Mech. Mater. Struct.*, **2**(7), 1381-1394. https://doi.org/10.2140/jomms.2007.2.1381.
Liu, I.W. and Lin, C.C. (1991), "Optimum design of composite wing structures by a refined optimality criterion", *Compos. Struct.*, **17**(1), 51-65. https://doi.org/10.1016/0263-8223(91)90060-C.
Maalawi, K. (2011), "Functionally graded bars with enhanced dynamic performance", *J. Mech. Mater. Struct.*, **6**(1), 377-393. http://doi.org/10.2140/jomms.2011.6.377.
Mazidi, A. and Fazelzadeh, S.A. (2010), "Flutter of a swept aircraft wing with a powered engine", *J. Aerosp. Eng.*, **23**(4), 243-250. http://doi.org/10.1061/(ASCE)AS.1943-5525.0000037.
Mehri, M., Asadi, H. and Kouchakzadeh, M.A. (2017), "Computationally efficient model for flow-induced instability of CNT reinforced functionally graded truncated conical curved panels subjected to axial compression", *Comput. Meth. Appl. Mech. Eng.*, **318**, 957-980. https://doi.org/10.1016/j.cma.2017.02.020.
Patil, M. (1997), "Aeroelastic tailoring of composite box beams", *Proceedings of the 35th Aerospace Sciences Meeting and Exhibit*, American Institute of Aeronautics and Astronautics, Reno, Nevada, U.S.A., January.
Qin, Z. and Librescu, L. (2003), "Aeroelastic instability of aircraft wings modelled as anisotropic composite thin-walled beams in incompressible flow", *J. Fluid. Struct.*, **18**(1), 43-61. http://doi.org/10.1016/S0889-9746(03)00082-3.
Sayadi, M.K., Hafezalkotob, A. and Naini, S.G.J. (2013), "Firefly-inspired algorithm for discrete optimization problems: An application to manufacturing cell formation", *J. Manuf. Syst.*, **32**(1), 78-84. https://doi.org/10.1016/j.jmsy.2012.06.004.
Shukla, R. and Singh, D. (2017), "Selection of parameters for advanced machining processes using firefly algorithm", *Eng. Sci. Technol.*, **20**(1), 212-221. https://doi.org/10.1016/j.jestch.2016.06.001.
Sommerwerk, K., Michels, B., Lindhorst, K., Haupt, M.C. and Horst, P. (2016), "Application of efficient surrogate modeling to aeroelastic analyses of an aircraft wing", *Aerosp. Sci. Technol.*, **55**, 314-323. https://doi.org/10.1016/j.ast.2016.06.011,
Song, Z., Chen, Y., Li, Z., Sha, J. and Li, F. (2019), "Axially functionally graded beams and panels in supersonic airflow and their excellent capability for passive flutter suppression", *Aerosp. Sci. Technol.*, **92**, 668-675. https://doi.org/10.1016/j.ast.2019.06.042.
Tsiatas, G.C. and Charalampakis, A.E. (2017), "Optimizing the natural frequencies of axially functionally graded beams and arches", *Compos. Struct.*, **160**, 256-266. https://doi.org/10.1016/j.compstruct.2016.10.057.
Wan, Z., Yan, H., Liu, D. and Yang, C. (2005), "Aeroelastic analysis and optimization of high-aspect-ratio composite forward-swept wings", *Chin. J. Aeronaut.*, **18**(4), 317-325. https://doi.org/10.1016/S1000-9361(11)60251-3.

Weisshaar, T.A. (1981), "Aeroelastic tailoring of forward swept composite wings", *J. Aircraft*, **18**(8), 669-676. https://doi.org/10.2514/3.57542.
Ziane, N., Meftah, S.A., Belhadj, H.A., Tounsi, A. and Bedia, E.A.A. (2013), "Free vibration analysis of thin and thick-walled FGM box beams", *Int. J. Mech. Sci.*, **66**, 273-282. https://doi.org/10.1016/j.ijmecsci.2012.12.001.

GY